

# Running the running

Giovanni Cabass,<sup>1</sup> Eleonora Di Valentino,<sup>2</sup> Alessandro Melchiorri,<sup>1</sup> Enrico Pajer,<sup>3</sup> and Joseph Silk<sup>2,4,5,6</sup>

<sup>1</sup>*Physics Department and INFN, Università di Roma “La Sapienza”, P.le Aldo Moro 2, 00185, Rome, Italy*

<sup>2</sup>*Institut d’Astrophysique de Paris (UMR7095: CNRS & UPMC-Sorbonne Universities), F-75014, Paris, France*

<sup>3</sup>*Institute for Theoretical Physics and Center for Extreme Matter and Emergent Phenomena, Utrecht University, Princetonplein 5, 3584 CC Utrecht, The Netherlands*

<sup>4</sup>*AIM-Paris-Saclay, CEA/DSM/IRFU, CNRS, Univ. Paris VII, F-91191 Gif-sur-Yvette, France*

<sup>5</sup>*Department of Physics and Astronomy, The Johns Hopkins University Homewood Campus, Baltimore, MD 21218, USA*

<sup>6</sup>*BIPAC, Department of Physics, University of Oxford, Keble Road, Oxford OX1 3RH, UK*

We use the recent observations of Cosmic Microwave Background temperature and polarization anisotropies provided by the *Planck* satellite experiment to place constraints on the running  $\alpha_s = dn_s/d \log k$  and the running of the running  $\beta_s = d\alpha_s/d \log k$  of the spectral index  $n_s$  of primordial scalar fluctuations. We find  $\alpha_s = 0.011 \pm 0.010$  and  $\beta_s = 0.027 \pm 0.013$  at 68% CL, suggesting the presence of a running of the running at the level of two standard deviations. We find no significant correlation between  $\beta_s$  and foregrounds parameters, with the exception of the point sources amplitude at 143 GHz,  $A_{143}^{PS}$ , which shifts by half sigma when the running of the running is considered. We further study the cosmological implications of such preference for  $\alpha_s, \beta_s \sim 0.01$  by including in the analysis the lensing amplitude  $A_L$ , the curvature parameter  $\Omega_k$ , and the sum of neutrino masses  $\sum m_\nu$ . We find that when the running of the running is considered, *Planck* data are more compatible with the standard expectations of  $A_L = 1$  and  $\Omega_k = 0$  but still hint at possible deviations. The indication for  $\beta_s > 0$  survives at two standard deviations when external datasets such as BAO and CFHTLenS are included in the analysis, and persists at  $\sim 1.7$  standard deviations when CMB lensing is considered. We discuss the possibility of constraining  $\beta_s$  with current and future measurements of CMB spectral distortions, showing that an experiment like PIXIE could provide strong constraints on  $\alpha_s$  and  $\beta_s$ .

PACS numbers: 98.80.Es, 98.80.Cq

## I. INTRODUCTION

The recent measurement of the Cosmic Microwave Background (CMB) anisotropies provided by the *Planck* satellite mission (see [1, 2], for example) have provided a wonderful confirmation of the standard  $\Lambda$ CDM cosmological model. However, when the base model is extended and other cosmological parameters are let free to vary, a few “anomalies” are present in the parameter values that, even if their significance is only at the level of two standard deviations, deserve further investigation.

First of all, the parameter  $A_L$ , that measures the amplitude of the lensing signal in the CMB angular spectra [3], has been found larger than the standard value with  $A_L = 1.22 \pm 0.10$  at 68% CL ( $A_L = 1$  being the expected value in  $\Lambda$ CDM) from *Planck* temperature and polarization angular spectra [1]. A value of  $A_L$  larger than one is difficult to accommodate in  $\Lambda$ CDM, and several solutions have been proposed as modified gravity [4, 5], neutrino anisotropies [6], and compensated isocurvature perturbations [7]. Combining *Planck* with data from the Atacama Cosmology Telescope (ACT) and the South Pole Telescope (SPT) to better constrain the foregrounds, Couchot et al. [8], found a consistency with  $A_L = 1$ . However the compatibility of the CMB datasets used is unclear. More recently Addison et al. [9] have found that including the  $A_L$  parameter solves the tension between *Planck* and WMAP9 on the value of the derived cosmological parameters.

As shown in [1], the  $A_L$  anomaly persists when the

*Planck* data is combined with Baryonic Acoustic Oscillation surveys (BAO), it is enhanced when the CFHTLenS shear lensing survey is included, but it practically disappears when CMB lensing from *Planck* trispectrum observations are considered. The  $A_L$  anomaly is also still present in a 12-parameter extended  $\Lambda$ CDM analysis of the *Planck* dataset (see [10]), showing no significant correlation with extra parameters such as the dark energy equation of state  $w$ , the neutrino mass, and the neutrino effective number  $N_{\text{eff}}$ .

Second, the *Planck* dataset prefers a positively curved universe, again at about two standard deviations with  $\Omega_k = -0.040 \pm 0.020$  at 68% CL. This “anomaly” is not due to an increased parameter volume effect but, as stated in [2], curvature provides a genuine better fit to the data with an improved fit of  $\Delta\chi^2 \sim 6$ . When BAO data is included, however, the curvature of the universe is again compatible with zero with the stringent constraint  $\Omega_k = -0.000 \pm 0.005$  at 95% CL.

The fact that both the  $A_L$  and  $\Omega_k$  anomalies disappear when reliable external datasets are included suggests that their origin might be a systematic or that they are produced by a different physical effect than lensing or curvature.

In this respect it is interesting to note that a third parameter is constrained to anomalous values from the *Planck* data. The primordial scalar spectral index  $n_s$  of scalar perturbations is often assumed to be independent of scale. However, since some small scale-dependence is

expected,<sup>1</sup> we can expand the dimensionless scalar power spectrum  $\Delta_{\zeta}^2(k) = k^3 P_{\zeta}(k)/2\pi^2$  as

$$\Delta_{\zeta}^2(k) = A_s \left( \frac{k}{k_*} \right)^{n_s - 1 + \frac{\alpha_s}{2} \log \frac{k}{k_*} + \frac{\beta_s}{6} \left( \log \frac{k}{k_*} \right)^2}, \quad (1)$$

where  $\alpha_s$  is the running of the spectral index,  $\beta_s$  is the running of the running, and  $k_* = 0.05 \text{ Mpc}^{-1}$ .

The *Planck* temperature and polarization data analysis presented in [2], while providing a small indication for a *positive* running different from zero ( $\alpha_s = 0.009 \pm 0.010$  at 68% CL), suggests also the presence of a running of the running at the level of two standard deviations ( $\beta_s = 0.025 \pm 0.013$  at 68% CL). The inclusion of a running of the running improves the fit to the *Planck* temperature and polarization data by  $\Delta\chi^2 \sim 5$  with respect to the  $\Lambda$ CDM model. Therefore we do not expect that such anomaly is due to the increased parameter volume, and could be a hint of possible new physics beyond the standard model. A discussion of the impact of this anomaly on inflationary models has been presented in [11, 12].

Given this result, it is timely to discuss the possible correlations between these three anomalies,  $\beta_s$ ,  $A_L$  and  $\Omega_k$  and see, for example, if one of them vanishes if a second one is considered at the same time in the analysis. Moreover (related to the above points), it is necessary to investigate in more detail how the inclusion of  $\beta_s$  helps giving a better fit to the data, and test if the indication for the running of the running survives when additional datasets as BAO or lensing (CMB and shear) are considered. This is the goal of this paper.

We structure the discussion as follows. In the next section we will describe the analysis method and the cosmological datasets used. In Sec. III we present our results and discuss possible correlations between  $\beta_s$ ,  $A_L$  and  $\Omega_k$ . We also investigate the possibility that a running of the running affects current and future measurements of CMB spectral distortions, comparing our results with those of [13]. Finally, in Sec. VI we derive our conclusions.

## II. METHOD

We perform a Monte Carlo Markov Chain (MCMC) analysis of the most recent cosmological datasets using the publicly available code `cosmomc` [14, 15]. We consider the 6 parameters of the standard  $\Lambda$ CDM model, *i.e.* the baryon  $\omega_b \equiv \Omega_b h^2$  and cold dark matter  $\omega_c \equiv \Omega_c h^2$  energy densities, the angular size of the horizon at the last scattering surface  $\theta_{\text{MC}}$ , the optical depth  $\tau$ , the amplitude of primordial scalar perturbations  $\log(10^{10} A_s)$  and the scalar spectral index  $n_s$ . We extend this scenario by

including the running of the scalar spectral index  $\alpha_s$  and the running of the running  $\beta_s$ . We fix the pivot scale at  $k_* = 0.05 \text{ Mpc}^{-1}$ . This is our baseline cosmological model, that we will call “base” in the following. Moreover, as discussed in the introduction, we also consider separate variation in the lensing amplitude  $A_L$ , in the curvature density  $\Omega_k$  and in the sum of neutrino masses  $\sum m_\nu$ .

The main dataset we consider, to which we refer as “*Planck*”, is based on CMB temperature and polarization anisotropies. We analyze the temperature and polarization *Planck* likelihood [16]: more precisely, we make use of the *TT*, *TE*, *EE* high- $\ell$  likelihood together with the *TEB* pixel-based low- $\ell$  likelihood. The additional datasets we consider are the following:

- *Planck* measurements of the lensing potential power spectrum  $C_{\ell}^{\phi\phi}$  [17];
- weak gravitational lensing data of the CFHTLenS survey [18, 19], taking only wavenumbers  $k \leq 1.5h \text{ Mpc}^{-1}$  [1, 20];
- Baryon Acoustic Oscillations (BAO): the surveys included are 6dFGS [21], SDSS-MGS [22], BOSS LOWZ [23] and CMASS-DR11 [23]. This dataset will help to break geometrical degeneracies when we let  $\Omega_k$  free to vary.

## III. RESULTS

In Tab. I we present the constraints on  $n_s$ ,  $\alpha_s$  and  $\beta_s$  from the *Planck* 2015 temperature and polarization data and in combination with BAO, cosmic shear and CMB lensing. As we can see, the *Planck* alone dataset provides an indication for  $\beta_s > 0$  at more than two standard deviations with  $\beta_s = 0.027 \pm 0.013$  at 68% CL.

It is interesting to investigate the impact of the inclusion of  $\alpha_s$  and  $\beta_s$  on the remaining 6 parameters of the  $\Lambda$ CDM model. Comparing our results with those reported in Table 3 of [2], we see that there are no major shifts on the parameters. The largest shifts are present for the scalar spectral index  $n_s$ , that is  $\sim 0.9$  standard deviations *lower* when  $\beta_s$  is included, and for the reionization optical depth  $\tau$  that is  $\sim 0.9$  standard deviations *higher* with respect to the standard  $\Lambda$ CDM scenario. A similar shift is also present for the value of the root mean square density fluctuations on scales of  $8h \text{ Mpc}^{-1}$  (the  $\sigma_8$  derived parameter), which is higher by about one standard deviation when  $\beta_s$  is considered. In Fig. 1 we plot the probability contour at 68% CL and 95% CL for the several combinations of datasets in the  $\beta_s - \sigma_8$  and  $\beta_s - \tau$  planes respectively. Clearly, a new determination of  $\tau$  from future large-scale polarization data as those expected from the *Planck* HFI experiment could have an impact on the value of  $\beta_s$ . On the other hand, this one sigma shift in  $\tau$  with respect to  $\Lambda$ CDM shows that a

<sup>1</sup> *E.g.*, we expect a running of the tilt  $n_s$  of order  $(1 - n_s)^2$  in slow-roll inflation.

base	<i>Planck</i>	+ lensing	+ WL	+ BAO
$\Omega_b h^2$	$0.02216 \pm 0.00017$	$0.02215 \pm 0.00017$	$0.02221 \pm 0.00017$	$0.02224 \pm 0.00015$
$\Omega_c h^2$	$0.1207 \pm 0.0015$	$0.1199 \pm 0.0015$	$0.1197 \pm 0.0014$	$0.1196 \pm 0.0011$
$100\theta_{\text{MC}}$	$1.04070 \pm 0.00032$	$1.04080 \pm 0.00032$	$1.04078 \pm 0.00032$	$1.04082^{+0.00029}_{-0.00030}$
$\tau$	$0.091 \pm 0.019$	$0.064 \pm 0.014$	$0.086 \pm 0.019$	$0.096 \pm 0.018$
$H_0$	$66.88 \pm 0.68$	$67.16 \pm 0.67$	$67.29^{+0.66}_{-0.65}$	$67.36^{+0.49}_{-0.48}$
$\log(10^{10} A_s)$	$3.118 \pm 0.037$	$3.061 \pm 0.026$	$3.104^{+0.038}_{-0.037}$	$3.125 \pm 0.036$
$n_s$	$0.9582^{+0.0055}_{-0.0054}$	$0.9607 \pm 0.0054$	$0.9608 \pm 0.0055$	$0.9613^{+0.0046}_{-0.0047}$
$\alpha_s$	$0.011 \pm 0.010$	$0.012 \pm 0.010$	$0.012 \pm 0.010$	$0.010 \pm 0.010$
$\beta_s$	$0.027 \pm 0.013$	$0.022 \pm 0.013$	$0.026 \pm 0.013$	$0.025 \pm 0.013$

TABLE I. 68% CL bounds on  $\Omega_b h^2$ ,  $\Omega_c h^2$ ,  $100\theta_{\text{MC}}$ ,  $\tau$ ,  $H_0$ ,  $\log(10^{10} A_s)$ ,  $n_s$ ,  $\alpha_s$ ,  $\beta_s$ , for the listed datasets: the model is  $\Lambda\text{CDM} + \alpha_s + \beta_s$ ,  $k_* = 0.05 \text{ Mpc}^{-1}$ .

large-scale measurement of CMB polarization does not fully provide a direct determination of  $\tau$  but that some model dependence is present.

Moreover, as expected, there is a strong correlation between  $\alpha_s$  and  $\beta_s$ . Because of this correlation, the running  $\alpha_s$  is constrained to be positive, with  $\alpha_s > 0$  at more than 68% CL when  $\beta_s$  is considered. This is a  $\sim 1.3$  standard deviations shift on  $\alpha_s$  if we compare this result with the value obtained using the same dataset but fixing  $\beta_s = 0$  in Table 5 of [2]. In Fig. 2 we plot the two dimensional likelihood constraints in the  $n_s - \beta_s$  and  $\alpha_s - \beta_s$  planes respectively. As we can see, a correlation between the parameters is clearly present. However, when  $\alpha_s$  and possibly higher derivatives of the scalar tilt are left free to vary, the constraints will depend on the choice of the pivot scale  $k_*$  [24]. We have therefore considered two additional values of  $k_*$ , *i.e.*  $k_* = 0.01 \text{ Mpc}^{-1}$  and  $k_* = 0.002 \text{ Mpc}^{-1}$ : the resulting plots are shown in Sec. VII A (where we also present a simple argument to explain the stability of  $\sigma_{\beta_s}$  under change of  $k_*$ ), while Tab. II shows the 68% CL constraints on  $n_s$ ,  $\alpha_s$  and  $\beta_s$  (“base” model, *Planck TT, TE, EE + lowP* dataset<sup>2</sup>). From Tab. II we see that, while the  $1\sigma$  indication for  $\alpha_s > 0$  disappears if we change  $k_*$  (becoming a  $\sim 2\sigma$  evidence for negative running),  $\beta_s$  remains larger than 0 at  $\sim 2\sigma$ .<sup>3</sup> We therefore conclude that the preference for blue  $\beta_s$  is stable under the variation of  $k_*$ : by studying the improvement in  $\chi^2$  with respect to the  $\Lambda\text{CDM}$  and  $\Lambda\text{CDM} + \alpha_s$  models, we can understand what is its origin.

The *Planck* likelihood consists essentially of three terms: a low- $\ell$  ( $\ell = 2 \div 29$ ) TEB likelihood based on the *Planck* LFI 70 GHz channel full mission dataset, an

base	$k_* = 0.01 \text{ Mpc}^{-1}$	$k_* = 0.002 \text{ Mpc}^{-1}$
$n_s$	$0.9758^{+0.0117}_{-0.0116}$	$1.0632^{+0.0466}_{-0.0459}$
$\alpha_s$	$-0.032 \pm 0.015$	$-0.076 \pm 0.035$
$\beta_s$	$0.027 \pm 0.013$	$0.027 \pm 0.013$

TABLE II. 68% CL constraints on  $n_s$ ,  $\alpha_s$ ,  $\beta_s$ , for the listed pivot scales: the model is  $\Lambda\text{CDM} + \alpha_s + \beta_s$ , and the dataset is *Planck (TT, TE, EE + lowP)*.

high- $\ell$  likelihood based on *Planck* HFI 100 GHz, 143 GHz and 217 GHz channels half mission dataset and, finally, an additional  $\chi^2$  term that comes from the external priors assumed on foregrounds (see [16]). By looking at the mean  $\chi_{\text{eff}}^2$  values from these three terms we can better understand from where (low  $\ell$ , high  $\ell$ , foregrounds) the indication for  $\beta_s$  is coming. Comparing with the  $\chi^2$  values obtained under standard  $\Lambda\text{CDM}$  with  $\alpha_s = 0$  and  $\beta_s = 0$ , we have found that while the high- $\ell$  likelihood remains unchanged, there is an improvement in the low- $\ell$  likelihood of  $\Delta\chi_{\text{eff}}^2 \sim 2.5$  and in the foregrounds term with  $\Delta\chi_{\text{eff}}^2 \sim 1$ . The inclusion of  $\beta_s$  provides therefore a better fit to the low- $\ell$  part of the CMB spectrum and to the foregrounds prior. While the better fit to the low- $\ell$  part of the CMB spectrum can be easily explained by the low quadrupole *TT* anomaly and by the dip at  $\ell \sim 20-30$ , the change due to foregrounds is somewhat unexpected since, in general, foregrounds do not correlate with cosmological parameters. We have found a significant correlation between  $\beta_s$  and the point source amplitude at 143 GHz,  $A_{143}^{PS}$ . The posterior of  $A_{143}^{PS}$  shifts indeed by half sigma towards lower values with respect to the standard  $\Lambda\text{CDM}$  case (see Fig. 3) from  $A_{143}^{PS} = 43 \pm 8$  to  $A_{143}^{PS} = 39 \pm 8$  at 68% CL. This shift could also explain the small difference between the constraints reported here and those reported in [2], that uses the *Pliklite* likelihood code where fore-

<sup>2</sup> A study of the impact of  $k_*$  when also  $A_L$ ,  $\sum m_\nu$  and  $\Omega_K$  are varied is left to future work.

<sup>3</sup> We also note a  $\sim 1\sigma$  indication of blue tilt when  $k_*$  is  $0.002 \text{ Mpc}^{-1}$ .

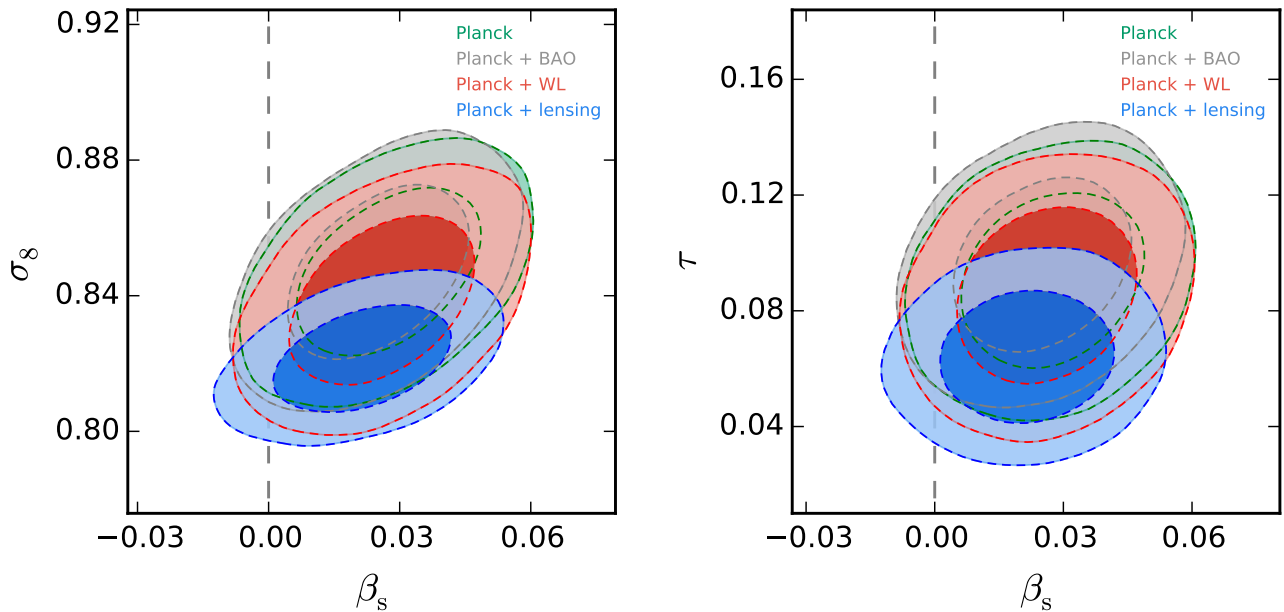


FIG. 1. Constraints at 68% CL and 95% CL in the  $\beta_s - \sigma_8$  plane (left panel) and in the  $\beta_s - \tau$  plane (right panel).

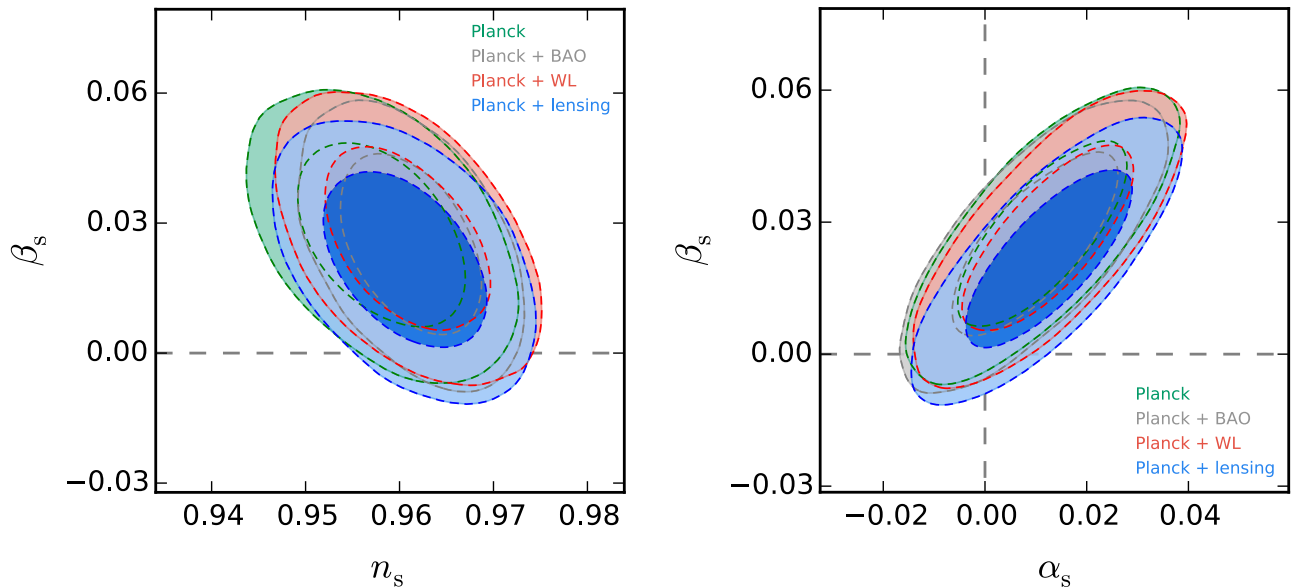


FIG. 2. Likelihood constraints in the  $n_s - \beta_s$  (left panel) and  $\alpha_s - \beta_s$  (right panel) planes for different combination of datasets, as discussed in the text.

grounds are marginalized at their  $\Lambda$ CDM values.

Before proceeding, we stress that using a likelihood ratio test [25] it is easy to see that, for a  $\Delta\chi_{\text{eff}}^2 \sim 3.5$  (as the one we find here), there still is a  $\sim 17\%$  probability that

the  $\Lambda$ CDM model is the correct one.<sup>4</sup> Given the *Planck*  $TT$ ,  $TE$ ,  $EE$  + lowP dataset, this is the significance with which the  $\Lambda$ CDM +  $\alpha_s$  +  $\beta_s$  model is preferred over the

<sup>4</sup> Using the fact that  $2\log(\mathcal{L}_1/\mathcal{L}_2)$  is distributed as a  $\chi^2$  with  $\text{d.o.f.} = \text{d.o.f.}_1 - \text{d.o.f.}_2$ .

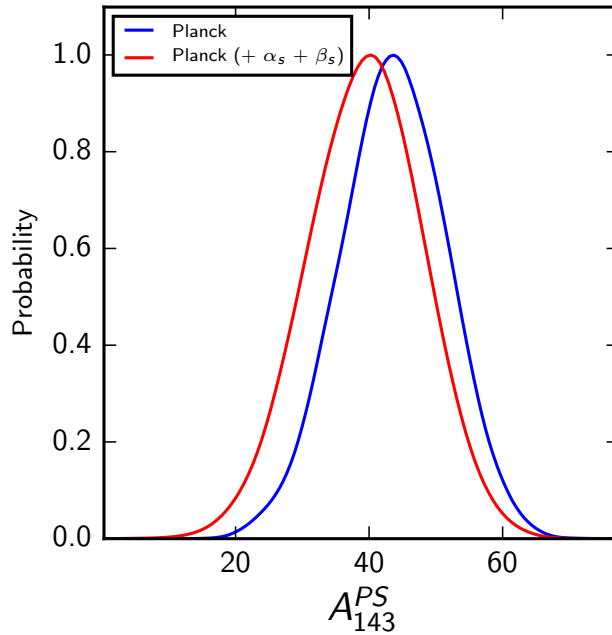


FIG. 3. Shift in the amplitude of unresolved foreground point sources at 143 GHz between the  $\Lambda$ CDM case and the case when variation in  $\alpha_s$  and  $\beta_s$  are considered. The dataset used is *Planck* temperature and polarization angular spectra.

$\Lambda$ CDM one.

Going back to Tab. I, we can see that the indication for  $\beta_s > 0$  is slightly weakened but still present also when external datasets are considered. Adding CMB lensing gives  $\beta_s = 0.022 \pm 0.013$ , *i.e.* reducing the tension to about 1.7 standard deviations, while the inclusion of weak lensing and BAO data does not lead to an appreciable decrease in the statistical significance of  $\alpha_s$  and  $\beta_s$ .

In Tab. III we report similar constraints but including also variations in the neutrino mass absolute scale  $\sum m_\nu$ . The constraints obtained from the *Planck* 2015 data release on the neutrino masses are indeed very strong, especially when combined with BAO data, ruling out the possibility of a direct detection from current and future beta and double beta decay experiments (see, *e.g.*, [26]). Since *Planck* data show a preference for  $\beta_s > 0$ , it is clearly interesting to investigate if the inclusion of running has some impact on the cosmological constraints on  $\sum m_\nu$ . Comparing the results of Tab. III with those in [2], which were obtained assuming  $\alpha_s = \beta_s = 0$ , we see that the constraints on  $\sum m_\nu$  are only slightly weakened, moving from  $\sum m_\nu < 0.490$  eV to  $\sum m_\nu < 0.530$  eV at 95% CL for the *Planck* dataset alone and from  $\sum m_\nu < 0.590$  eV to  $\sum m_\nu < 0.644$  eV at 95% CL when also lensing is considered. The constraints on  $\sum m_\nu$  including the WL and BAO datasets are essentially unaffected by  $\beta_s$ . We can therefore conclude that there is no significant correlation between  $\beta_s$  and  $\sum m_\nu$ .

In Fig. 4 we plot the posterior distributions for  $\sum m_\nu$ , while in Fig. 5 we plot the probability contour at 68% CL and 95% CL for the several combinations of datasets in

the  $\beta_s - \sum m_\nu$  plane, respectively.

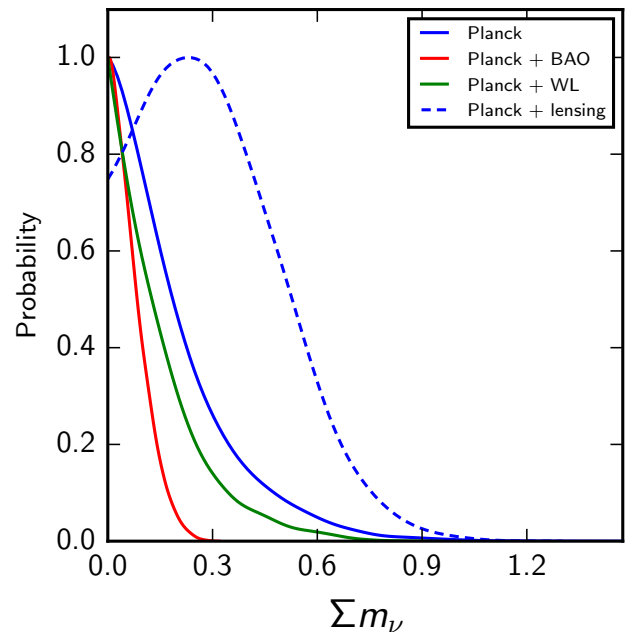


FIG. 4. One-dimensional posterior distributions for the sum of neutrino masses  $\sum m_\nu$ , for the indicated datasets. The model considered is  $\Lambda$ CDM +  $\alpha_s + \beta_s + \sum m_\nu$ .

In Tab. IV we report the constraints from the same datasets but letting also the lensing amplitude  $A_L$  free to vary. As discussed in the introduction, *Planck* data are

base + $\sum m_\nu$	<i>Planck</i>	+ lensing	+ WL	+ BAO
$\Omega_b h^2$	$0.02213 \pm 0.00018$	$0.02207 \pm 0.00019$	$0.02219 \pm 0.00018$	$0.02224 \pm 0.00015$
$\Omega_c h^2$	$0.1208 \pm 0.0016$	$0.1206 \pm 0.0016$	$0.1199 \pm 0.0015$	$0.1196 \pm 0.0011$
$100\theta_{\text{MC}}$	$1.04062^{+0.00033}_{-0.00034}$	$1.04060 \pm 0.00035$	$1.04072 \pm 0.00033$	$1.04082 \pm 0.00030$
$\tau$	$0.095^{+0.019}_{-0.020}$	$0.080 \pm 0.019$	$0.088 \pm 0.020$	$0.095^{+0.020}_{-0.019}$
$(\sum m_\nu)/\text{eV}$	$< 0.530$	$< 0.644$	$< 0.437$	$< 0.159$
$H_0$	$65.76^{+2.12}_{-0.99}$	$64.76^{+2.49}_{-1.70}$	$66.46^{+1.76}_{-0.91}$	$67.38 \pm 0.56$
$\log(10^{10} A_s)$	$3.127^{+0.038}_{-0.039}$	$3.093^{+0.037}_{-0.036}$	$3.109 \pm 0.038$	$3.124^{+0.037}_{-0.038}$
$n_s$	$0.9576^{+0.0056}_{-0.0057}$	$0.9583 \pm 0.0057$	$0.9601^{+0.0055}_{-0.0054}$	$0.9612^{+0.0047}_{-0.0048}$
$\alpha_s$	$0.011 \pm 0.010$	$0.011 \pm 0.010$	$0.012 \pm 0.010$	$0.010^{+0.010}_{-0.011}$
$\beta_s$	$0.028 \pm 0.013$	$0.023 \pm 0.013$	$0.026 \pm 0.013$	$0.025 \pm 0.013$

TABLE III. 68% CL bounds and 95% CL upper limits on  $\Omega_b h^2$ ,  $\Omega_c h^2$ ,  $100\theta_{\text{MC}}$ ,  $\tau$ ,  $\sum m_\nu$ ,  $H_0$ ,  $\log(10^{10} A_s)$ ,  $n_s$ ,  $\alpha_s$ ,  $\beta_s$ , for the listed datasets: the model is  $\Lambda\text{CDM} + \alpha_s + \beta_s + \sum m_\nu$ ,  $k_\star = 0.05 \text{ Mpc}^{-1}$ .

base + $A_L$	<i>Planck</i>	+ lensing	+ WL	+ BAO
$\Omega_b h^2$	$0.02227 \pm 0.00019$	$0.02214 \pm 0.00018$	$0.02235 \pm 0.00019$	$0.02232 \pm 0.00016$
$\Omega_c h^2$	$0.1196 \pm 0.0017$	$0.1202 \pm 0.0017$	$0.1185 \pm 0.0016$	$0.1190 \pm 0.0011$
$100\theta_{\text{MC}}$	$1.04081 \pm 0.00033$	$1.04076 \pm 0.00033$	$1.04093 \pm 0.00033$	$1.04089 \pm 0.00030$
$\tau$	$0.070 \pm 0.025$	$0.070 \pm 0.025$	$< 0.095$	$0.070^{+0.024}_{-0.026}$
$A_L$	$1.106^{+0.079}_{-0.090}$	$0.984^{+0.058}_{-0.064}$	$1.157^{+0.077}_{-0.086}$	$1.118^{+0.075}_{-0.084}$
$H_0$	$67.38 \pm 0.77$	$67.04^{+0.75}_{-0.76}$	$67.88 \pm 0.73$	$67.64^{+0.52}_{-0.53}$
$\log(10^{10} A_s)$	$3.073^{+0.050}_{-0.051}$	$3.074^{+0.050}_{-0.051}$	$3.044^{+0.044}_{-0.051}$	$3.072 \pm 0.049$
$n_s$	$0.9621 \pm 0.0062$	$0.9597 \pm 0.0061$	$0.9652^{+0.0059}_{-0.0060}$	$0.9637 \pm 0.0049$
$\alpha_s$	$0.010 \pm 0.010$	$0.012 \pm 0.010$	$0.010 \pm 0.010$	$0.009 \pm 0.010$
$\beta_s$	$0.021 \pm 0.014$	$0.024 \pm 0.014$	$0.018 \pm 0.013$	$0.019 \pm 0.013$

TABLE IV. 68% CL bounds and 95% CL upper limits on  $\Omega_b h^2$ ,  $\Omega_c h^2$ ,  $100\theta_{\text{MC}}$ ,  $\tau$ ,  $A_L$ ,  $H_0$ ,  $\log(10^{10} A_s)$ ,  $n_s$ ,  $\alpha_s$ ,  $\beta_s$ , for the listed datasets: the model is  $\Lambda\text{CDM} + \alpha_s + \beta_s + A_L$ ,  $k_\star = 0.05 \text{ Mpc}^{-1}$ .

also suggesting a value for  $A_L > 1$  and is therefore interesting to check if there is a correlation with  $\beta_s$ . As we can see there is a correlation between the two parameters but not extremely significant. Even with a lower statistical significance, at about  $\sim 1.2 - 1.5$  standard deviations for  $A_L$  and  $\beta_s$  respectively (that could be also explained by the increased volume of parameter space), data seem to suggest the presence of *both* anomalies. When the CMB lensing data are included,  $A_L$  goes back to its standard value while the indication for  $\beta_s$  increases. When the WL shear data are included the  $A_L$  anomaly is present while the indication for  $\beta_s$  is weakened.

We also consider variation in the curvature of the universe and we report the constraints in Tab. V. As we can see, also in this case we have a correlation between  $\beta_s$  and  $\Omega_k$  but not significant enough to completely cancel

any indication for these anomalies from *Planck* data. Indeed, when  $\Omega_k$  is considered, we have still a preference for  $\Omega_k < 0$  and  $\beta_s > 0$  at more than one standard deviation. More interestingly, when external datasets are included, the indication for a positive curvature simply vanishes, while we get  $\beta_s > 0$  slightly below 95% CL.

In Fig. 6 we show the constraints at 68% CL and 95% CL in the  $\beta_s - A_L$  plane (left panel) and in the  $\beta_s - \Omega_k$  plane (right panel).

We conclude this section by looking at what are the improvements (or non-improvements) in  $\chi^2$  over our base model  $\Lambda\text{CDM} + \alpha_s + \beta_s$  when additional parameters ( $A_L$ ,  $\sum m_\nu$  and  $\Omega_K$ ) are considered: the tables (Tabs. VII, VIII, IX and X) containing all the  $\Delta\chi^2$  (which we define by  $\chi_{\text{base}}^2 - \chi_{\text{base} + \text{ext.}}^2$ ) are collected in Sec. VII B. When considering the  $+ A_L$  extension, we see that an

base + $\Omega_K$	<i>Planck</i>	+ lensing	+ WL	+ BAO
$\Omega_b h^2$	$0.02230 \pm 0.00019$	$0.02213 \pm 0.00018$	$0.02214 \pm 0.00019$	$0.02218 \pm 0.00018$
$\Omega_c h^2$	$0.1192^{+0.0017}_{-0.0018}$	$0.1204 \pm 0.0017$	$0.1206 \pm 0.0017$	$0.1205 \pm 0.0016$
$100\theta_{MC}$	$1.04086 \pm 0.00034$	$1.04074 \pm 0.00033$	$1.04068^{+0.00035}_{-0.00034}$	$1.04072^{+0.00033}_{-0.00034}$
$\tau$	$0.062^{+0.024}_{-0.028}$	$0.076 \pm 0.026$	$0.099^{+0.023}_{-0.024}$	$0.094 \pm 0.018$
$\Omega_K$	$-0.0302^{+0.0250}_{-0.0173}$	$0.0045^{+0.0096}_{-0.0076}$	$0.0082^{+0.0091}_{-0.0071}$	$0.0015 \pm 0.0021$
$H_0$	$57.75^{+4.81}_{-6.34}$	$69.71^{+4.11}_{-4.62}$	$71.70^{+3.91}_{-5.02}$	$67.72^{+0.71}_{-0.72}$
$\sigma_8$	$0.799^{+0.033}_{-0.036}$	$0.837 \pm 0.029$	$0.860^{+0.026}_{-0.027}$	$0.850 \pm 0.016$
$\log(10^{10} A_s)$	$3.057^{+0.048}_{-0.058}$	$3.087 \pm 0.052$	$3.133^{+0.047}_{-0.049}$	$3.124^{+0.036}_{-0.037}$
$n_s$	$0.9642^{+0.0064}_{-0.0065}$	$0.9589^{+0.0064}_{-0.0063}$	$0.9574 \pm 0.0063$	$0.9587 \pm 0.0057$
$\alpha_s$	$0.008^{+0.010}_{-0.011}$	$0.013 \pm 0.010$	$0.014 \pm 0.011$	$0.011 \pm 0.010$
$\beta_s$	$0.013 \pm 0.014$	$0.027^{+0.015}_{-0.017}$	$0.035^{+0.015}_{-0.017}$	$0.027 \pm 0.014$

TABLE V. 68% CL bounds on  $\Omega_b h^2$ ,  $\Omega_c h^2$ ,  $100\theta_{MC}$ ,  $\tau$ ,  $\Omega_K$ ,  $H_0$ ,  $\sigma_8$ ,  $\log(10^{10} A_s)$ ,  $n_s$ ,  $\alpha_s$ ,  $\beta_s$ , for the listed datasets: the model is  $\Lambda$ CDM +  $\alpha_s$  +  $\beta_s$  +  $\Omega_K$ ,  $k_* = 0.05 \text{ Mpc}^{-1}$ .

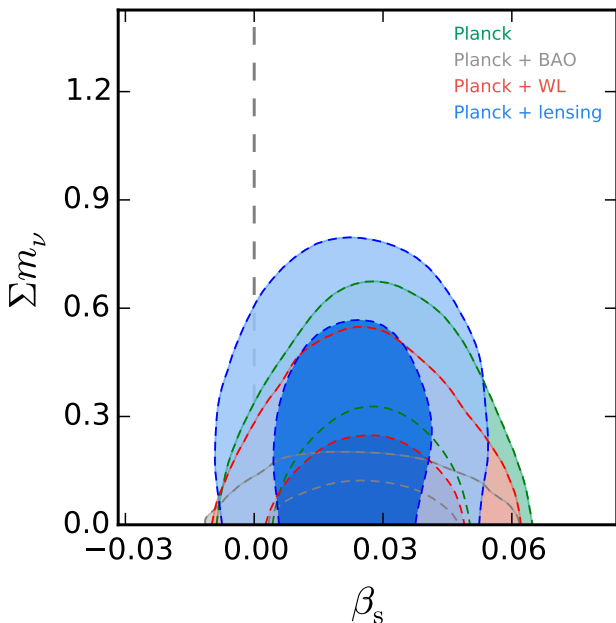


FIG. 5. Two-dimensional posteriors in the  $\beta_s - \sum m_\nu$  plane, for the indicated datasets. We see that there is no correlation between  $\sum m_\nu$  and  $\beta_s$ .

improvement  $\Delta\chi^2 \sim 1.5$  ( $\Delta\chi^2 \sim 6$ ) is obtained for the *Planck*  $TT$ ,  $TE$ ,  $EE$  + lowP + BAO dataset (*Planck*  $TT$ ,  $TE$ ,  $EE$  + lowP + WL dataset), while the addition of CMB lensing data to *Planck* temperature and polarization data leads to  $\Delta\chi^2 \sim -1.5$ , mainly driven by a worse fit to the foregrounds. When  $\sum m_\nu$  or  $\Omega_K$  are left free to vary, we see that the fit to the data is in general worse: only when adding  $\Omega_K$  to the *Planck*  $TT$ ,  $TE$ ,  $EE$

+ lowP + WL dataset we get a  $\Delta\chi^2 \sim 2$  improvement.

#### IV. PRESENT AND FUTURE CONSTRAINTS FROM $\mu$ -DISTORTIONS

CMB  $\mu$ -type spectral distortions [27, 28] from the dissipation of acoustic waves at redshifts between  $z = 2 \times 10^6 \equiv z_{dC}$  and  $z = 5 \times 10^4 \equiv z_{\mu-y}$  offer a window on the primordial power spectrum at very small scales, ranging from  $50$  to  $10^4 \text{ Mpc}^{-1}$  (for most recent works on this topic see [29–35] and references therein). The impact of a PIXIE-like mission on the constraints on the running  $\alpha_s$  has been recently analyzed in [34], while [31, 35] also investigated the variety of signals (and corresponding forecasts) that are expected in the  $\Lambda$ CDM model (not limited to a  $\mu$ -type distortion).

In this section, we briefly investigate the constraining power of  $\mu$ -distortions on  $\beta_s$ , given the *Planck* constraints on  $\alpha_s$  and  $\beta_s$  of Sec. III. We compute the contribution to the  $\mu$ -monopole from Silk damping of acoustic waves in the photon-baryon plasma [36–40], using the expression for the distortion visibility function presented in [31].<sup>5</sup> To understand the relationship between the  $\mu$  amplitude and the parameters of the primordial power spectrum, one can compute the (integrated) fractional energy that is dissipated by the acoustic waves  $\delta_\gamma$  between  $z = 2 \times 10^6$

<sup>5</sup> This is related to the method called “Method II” in [35], the difference being the visibility function  $J_{bb}(z)$  used:  $J_{bb}(z)$  is approximated to  $\exp(-(z/z_{dC})^{5/2})$  in the “Method II” of [35], while [31] derives a fitting formula to take into account the dependence of  $J_{bb}(z)$  on cosmological parameters. At the large values of  $\alpha_s$  and  $\beta_s$  allowed by *Planck*, we do not expect this difference to be very relevant for our final result.

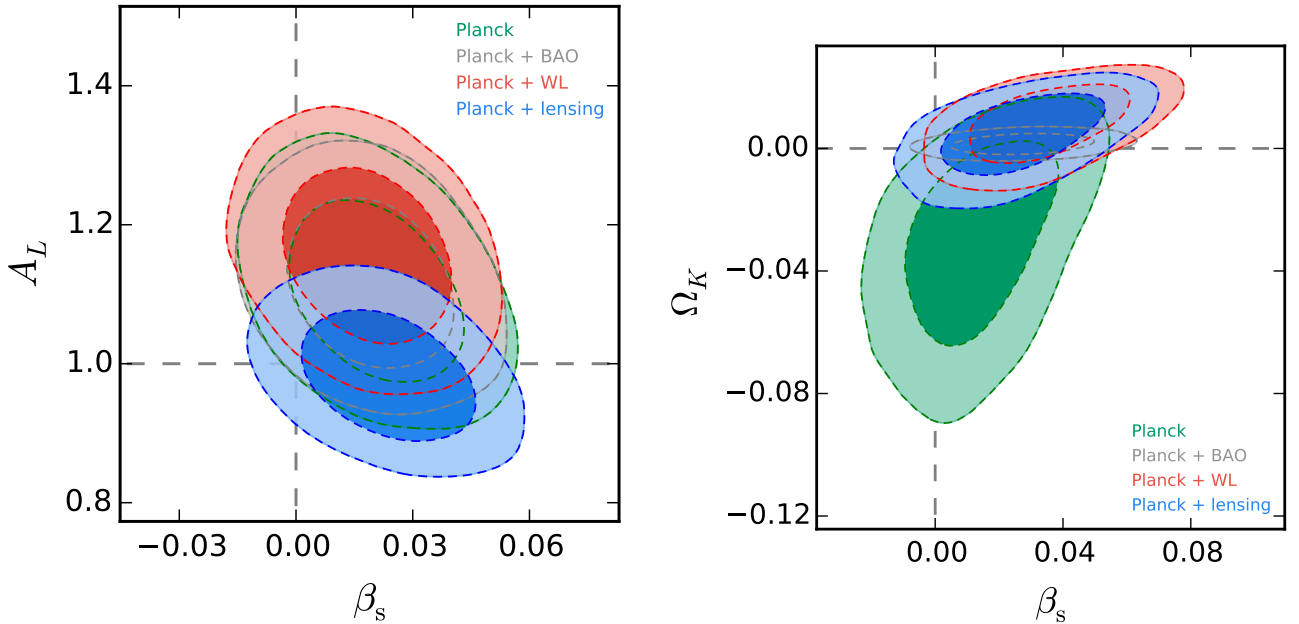


FIG. 6. Constraints at 68% CL and 95% CL in the  $\beta_s - A_L$  plane (left panel) and in the  $\beta_s - \Omega_k$  plane (right panel).

and  $z = 5 \times 10^4$ : this energy feeds back into the background and generates  $\mu$ -distortions according to (see also [41, 42])

$$\mu(\mathbf{x}) \approx \frac{1.4}{4} \langle \delta_\gamma^2(z, \mathbf{x}) \rangle_p \Big|_{z_{\mu-y}}^{z_{\text{dC}}}, \quad (2)$$

where  $\langle \dots \rangle_p$  indicates the average over a period of oscillation and  $\zeta$  is the primordial curvature perturbation. The diffusion damping length appearing in the above formula is given by [36–38]

$$k_D(z) = \sqrt{\int_z^{+\infty} dz \frac{1+z}{H n_e \sigma_T} \left[ \frac{R^2 + \frac{16}{15}(1+R)}{6(1+R)^2} \right]}. \quad (3)$$

The observed  $\mu$ -distortion monopole is basically the ensemble average of  $\mu(\mathbf{x})$  at  $z = 5 \times 10^4$ : by averaging Eq. (2), then, one sees that it is equal to the log-integral of the primordial power spectrum multiplied by a window function

$$W_\mu(k) = 2.3 e^{-2k^2/k_D^2} \Big|_{z_{\mu-y}}^{z_{\text{dC}}}, \quad (4)$$

which localizes the integral between  $50 \text{ Mpc}^{-1}$  to  $10^4 \text{ Mpc}^{-1}$ .

Tab. VI shows how, already with the current limit on the  $\mu$ -distortion amplitude from the FIRAS instrument on the COBE satellite, namely  $\mu = (1 \pm 4) \times 10^{-5}$  at 68% CL [43], we can get a 28% increase in the 95% CL upper limits on  $\alpha_s$ , and a 33% increase in those on  $\beta_s$  (we also stress that, in the case of  $\beta_s$  fixed to zero, including FIRAS does not result in any improvement on the bounds

for  $\alpha_s$ ). In Fig. 7, we also report a forecast for PIXIE, whose expected error on  $\mu$  is  $10^{-8}$  [44].<sup>6</sup> Besides, we see that:

- for the best-fit values of cosmological parameters in the  $\Lambda\text{CDM} + \alpha_s + \beta_s$  model, which leads to  $\mu = 1.09 \times 10^{-6}$ , PIXIE will be able to detect spectral distortions from Silk damping at extremely high significance (Fig. 7). Besides, we see that a statistically significant detection of  $\beta_s$  is expected, along with a sizable shrinking of the available parameter space (Fig. 7). As we discuss later, any detection of such values of  $\mu$ -distortions will rule out single-field slow-roll inflation, if we assume that all the generated distortions are due to Silk damping and not to other mechanisms like, for example, decaying Dark Matter particles;<sup>7</sup>

<sup>6</sup> In [45] it was shown that, when also  $r$ -distortions are considered, the expected error should be larger (about  $\sigma_\mu = 1.4 \times 10^{-8}$ ): however at the large values of  $\alpha_s$  and  $\beta_s$  allowed by *Planck*, the forecasts of Tab. VI are not significantly affected.  $r$ -distortions are the residual distortions that encode the information on the transition between the  $\mu$ -era (when distortions are of the  $\mu$ -type) and the  $y$ -era (when the CMB is not in kinetic equilibrium and energy injections result in distortions of the  $y$ -type). We refer to [46, 47] for a study of these residual distortions, and to [31, 45] for a study of their constraining power on cosmological parameters.

<sup>7</sup> We did not investigate, in this work, whether it could be possible to have models of multi-field inflation (or models where the slow-roll assumption is relaxed [48]) that can predict such values for the  $\mu$ -distortion amplitude. We refer to [32] for an analysis of some multi-field scenarios.

- for a fiducial value of  $\mu$  corresponding to the  $\Lambda$ CDM best-fit *i.e.*  $\mu = 1.57 \times 10^{-8}$  [34], we see that we get a 84% increase in the 95% CL upper limits on  $\alpha_s$ , and a 83% increase in those on  $\beta_s$ . More precisely, values of  $\beta_s$  larger than 0.02 will be excluded at  $\sim 5\sigma$ .

base	$\alpha_s$	$\beta_s$	$\mu$
<i>Planck</i>	$0.011 \pm 0.021$	$0.027 \pm 0.027$	/
+ FIRAS	$0.006^{+0.017}_{-0.018}$	$0.020^{+0.016}_{-0.019}$	$(0.77^{+3.10}_{-0.77}) \times 10^{-6}$
+ PIXIE	$-0.007^{+0.012}_{-0.013}$	$0.001^{+0.008}_{-0.009}$	$(1.59^{+1.75}_{-1.52}) \times 10^{-8}$

TABLE VI. 95% CL bounds on  $\alpha_s$  and  $\beta_s$  from the *Planck* (*TT*, *TE*, *EE* + lowP), *Planck* + FIRAS and *Planck* + PIXIE datasets, for the  $\Lambda$ CDM +  $\alpha_s$  +  $\beta_s$  (*i.e.* “base”) model. The results have been obtained by post-processing with a Gaussian likelihood the Markov chains considering  $\mu = (1.0 \pm 4.0) \times 10^{-5}$  [43] for FIRAS, and  $\mu = (1.57 \pm 1.00) \times 10^{-8}$  for PIXIE. See the main text for a discussion of the bounds on the  $\mu$ -amplitude.

We conclude this section with a comment on the validity of a Taylor expansion (in  $\log k/k_*$ ) of the power spectrum down to scales probed by spectral distortions. We can estimate the terms in the expansion of  $n_s(k)$  by choosing  $k = 10^4 \text{ Mpc}^{-1}$ , corresponding to  $k_D$  at  $z = z_{\text{dC}}$ : for values of  $\beta_s$  of order 0.06 (which are still allowed at 95% CL, as shown in Fig. 7), the term  $\frac{\beta_s}{6} (\log k/k_*)^2$  in Eq. (1) becomes of order 1. For this reason, Tab. VI does not report the limits on  $\mu$  coming from the current *Planck* constraints on the scale dependence of the spectrum. When existing limits on  $\mu$  from FIRAS are instead added, an extrapolation of  $\Delta_\zeta^2(k)$  at the scales probed by  $\mu$ -distortions starts to become meaningful, and when also PIXIE is included in our forecast around the  $\Lambda$ CDM prediction, the upper bounds on  $\alpha_s$  and  $\beta_s$  are lowered enough that a perturbative expansion becomes viable, making our forecast valid.

## V. LARGE $\beta_s$ AND SLOW-ROLL INFLATION

In this section we discuss briefly the implications that values of  $\alpha_s$  and  $\beta_s$  of order  $10^{-2}$  have for slow-roll inflation. We can compute the running of the slow-roll parameter  $\epsilon$  in terms of  $n_s$ ,  $\alpha_s$  and  $\beta_s$  by means of the simple slow-roll relations

$$N - N_* = -\log \frac{k}{k_*}, \quad (5a)$$

$$1 - n_s = 2\epsilon - \frac{1}{\epsilon} \frac{d\epsilon}{dN}, \quad (5b)$$

where  $N$  is the number of e-foldings from the end of inflation, decreasing as time increases (*i.e.*  $Hdt = -dN$ ), and Eq. (5a) holds if we neglect the time derivative of the inflaton speed of sound  $c_s$ . The running of  $\epsilon$  up to

third order in  $N$  is given, then, by

$$\epsilon(N) = \epsilon(N_*) + \sum_{i=1}^3 \frac{\epsilon^{(i)}}{i!} (N - N_*)^i, \quad (6)$$

where the coefficients  $\epsilon^{(i)}$  are given in Sec. VIII C.

At scales around  $k_*$ ,  $n_s$  dominates, so that  $\epsilon$  is increasing and a red spectrum is obtained. However, in presence of positive  $\alpha_s$  and  $\beta_s$ , at small scales  $\epsilon$  becomes smaller, until it becomes zero at  $k \approx 39.7 \text{ Mpc}^{-1}$  for  $\alpha_s = 0.01$  and  $\beta_s = 0.02$  (taking  $\epsilon_* = 0.002$ , *i.e.* the maximum value allowed by current bounds on  $r$ , when the inflaton speed of sound  $c_s$  is fixed to 1). If we impose that  $\epsilon$  stays positive down to  $k \approx 2 \times 10^4 \text{ Mpc}^{-1}$ , which is of the same order of magnitude of the maximum  $k$  probed by  $\mu$ -distortions (see Sec. IV), we can obtain a theoretical bound on  $\alpha_s$  and  $\beta_s$ . We show this bound in Fig. 7: this plot tells us that a large part of the contours from *Planck* + FIRAS and *Planck* + PIXIE cannot be interpreted in the context of slow-roll inflation extrapolated to  $\mu$ -distortion scales, because  $\epsilon$  becomes negative before reaching  $k \approx k_D(z_{\text{dC}})$ .<sup>8</sup>

A similar discussion was presented in [13]: by means of a slow-roll reconstruction of the inflaton potential [50, 51], it was shown that if  $\beta_s$  is controlled only by leading-order terms in the slow-roll expansion (see Sec. VII C), it is not possible to find a single-field inflation model that fits the posteriors from *Planck*.

These kind of bounds tell us that the Taylor expansion is not suitable for extrapolating the inflationary spectrum far away from the CMB window, in presence of the values of  $\alpha_s$  and  $\beta_s$  that are currently allowed by *Planck*, since  $\epsilon$  becomes zero already  $\sim 7$  e-folds after the horizon exit of  $k_*$ . To avoid this problem, one could consider a series expansion that takes into account the theoretical bounds on  $\epsilon$ , *i.e.*  $\epsilon(N=0) = 1$  and  $0 < \epsilon < 1$ : the Taylor series does not respect these requirements, so it does *not* in general represent a possible power spectrum from inflation, over the whole range of scales. Only when the values of the phenomenological parameters describing the scale dependence of the spectrum are small, the Taylor expansion can be a good approximation of a realistic power spectrum over a range of scales much larger than those probed by the CMB.

Another possibility is to consider bounds on the primordial power spectrum coming from observables that lie outside the CMB scales, but are still at small enough  $k$  that the Taylor series applies. These would be complementary to spectral distortions, which are basically sensitive only to scales around  $740 \text{ Mpc}^{-1}$  [30, 45], opening the possibility of multi-wavelength constraints on the scale dependence of the spectrum.

<sup>8</sup> We point out that it is possible to obtain large positive  $\alpha_s$  and  $\beta_s$  in slow-roll inflation when modulations of the potential are considered [49]. However, we will not consider such models in this work.

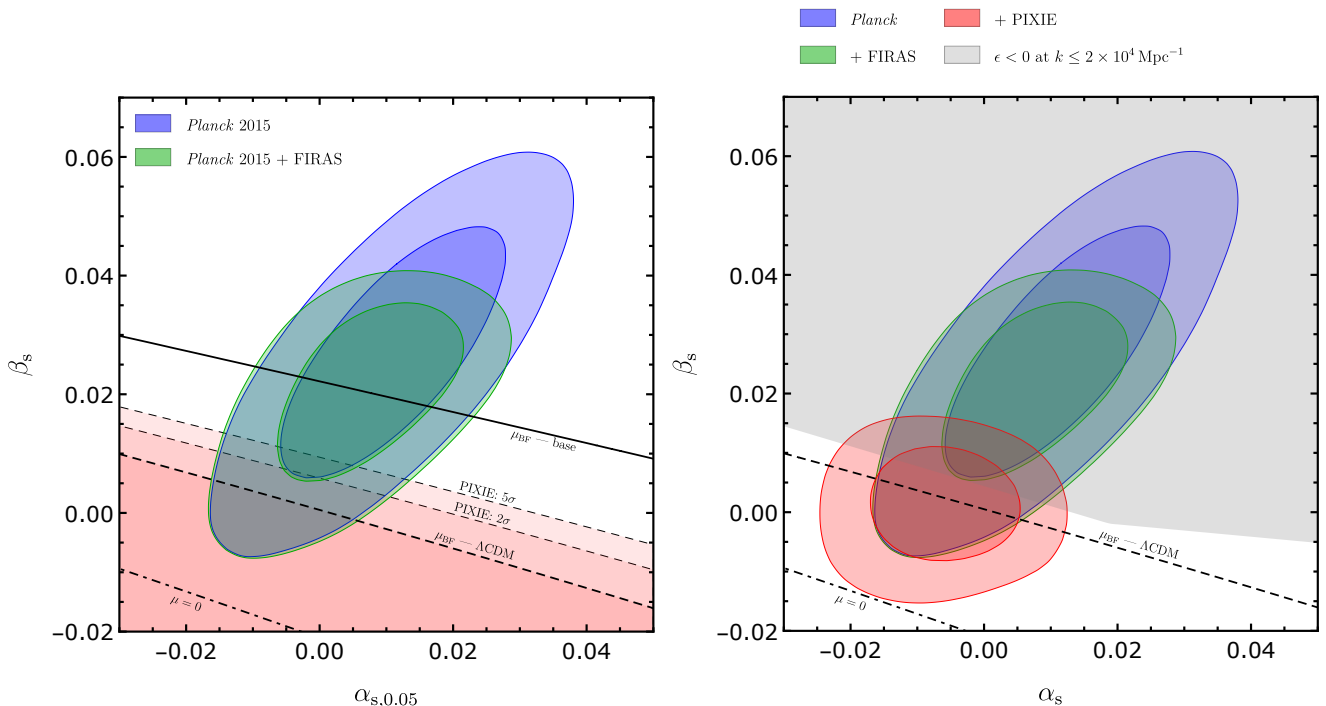


FIG. 7. Left panel: 68% CL and 95% CL contours in the  $\alpha_s - \beta_s$  plane, for the *Planck* (blue) and *Planck* + FIRAS (green) datasets (base model). The red regions represent the  $2\sigma$  and  $5\sigma$  limits from PIXIE around the *Planck* best-fit for the  $\Lambda\text{CDM}$  model, *i.e.*  $\mu = 1.57 \times 10^{-8}$  [34]. Right panel: same as left panel, with the red contours represent the 68% CL and 95% CL limits from PIXIE, obtained by post-processing the Markov chains with a Gaussian likelihood  $\mu = (1.57 \pm 1.00) \times 10^{-8}$ . The grey region represents the values of  $\alpha_s$  and  $\beta_s$  that lead to a slow-roll parameter  $\epsilon(k)$ , computed via the Taylor expansion of Eq. (6), less than zero before or at  $k = 2 \times 10^4 \text{ Mpc}^{-1}$ .

In this regard, observations of the Ly- $\alpha$  forest could be very powerful (the forest constrains wavenumbers  $k \approx 1 h \text{ Mpc}^{-1}$ ),<sup>9</sup> In [54], an analysis of the one-dimensional Ly- $\alpha$  forest power spectrum measured in [55] was carried out, showing that it provides also small-scale constraints on the tilt  $n_s$  and the running  $\alpha_s$ : more precisely, for a  $\Lambda\text{CDM} + \alpha_s + \sum m_\nu$  model, a detection at approximately  $3\sigma$  of  $\alpha_s$  ( $\alpha_s = -0.00135^{+0.0046}_{-0.0050}$  at 68% CL) is obtained. It would be interesting to carry out this analysis including the running of the running, to see if the bounds on  $\beta_s$  are also lowered.

## VI. CONCLUSIONS

In this paper we have presented new constraints on the running of the running of the scalar spectral index  $\beta_s$  and discussed in more detail the  $2\sigma$  indication for  $\beta_s > 0$  that comes from the analysis of CMB anisotropies data from the *Planck* satellite.

We have extended previous analyses by considering simultaneous variations in the lensing amplitude parameter  $A_L$  and the curvature of the universe  $\Omega_k$ . We have found that, while a correlation does exist between these parameters, *Planck* data still hint for non-standard values in the extended  $\Lambda\text{CDM} + \alpha_s + \beta_s + A_L$  and  $\Lambda\text{CDM} + \alpha_s + \beta_s + \Omega_k$  model, only partially suggesting a common origin for their anomalous signal related to the low CMB quadrupole. We have found that the *Planck* constraints on neutrino masses  $\sum m_\nu$  are essentially stable under the inclusion of  $\beta_s$ .

We have shown how future measurements of CMB  $\mu$ -type spectral distortions from the dissipation of acoustic waves, such as those expected by PIXIE, could severely constrain both the running and the running of the running. More precisely we have found that an improvement on *Planck* bounds by a factor of  $\sim 80\%$  is expected. Finally, we discussed the conditions under which the phenomenological expansion of the primordial power spectrum in Eq. (1) can be extended to scales much shorter than those probed by CMB anisotropies and can provide a good approximation to the predictions of inflationary models.

<sup>9</sup> Even if modeling the ionization state and thermodynamic properties of the intergalactic medium to convert flux measurements into a density power spectrum is very challenging (see [52] and [53] for a discussion).

## ACKNOWLEDGMENTS

We would like to thank Jens Chluba and Takeshi Kobayashi for careful reading of the manuscript and useful comments. We would also like to thank the referee for providing useful comments. GC and AM are supported by the research grant Theoretical Astroparticle Physics number 2012CPPYP7 under the program PRIN 2012 funded by MIUR and by TASP, iniziativa specifica INFN. EP is supported by the Delta-ITP consortium, a program of the Netherlands organization for scientific research (NWO) that is funded by the Dutch Ministry of Education, Culture and Science (OCW). This work has been done within the Labex ILP (reference ANR-10-LABX-63) part of the IDEX SUPER, and received financial state aid managed by the Agence Nationale de la Recherche, as part of the programme Investissements d’avenir under the reference ANR-11-IDEX-0004-02. EDV acknowledges the support of the European Research Council via the Grant number 267117 (DARK, P.I. Joseph Silk).

## VII. APPENDIX

### A. Dependence on the choice of pivot scale

When including derivatives of the scalar spectral index as free parameters, one can expect that the constraints on them will depend on the choice of pivot scale  $k_*$  [24]: for example, for *Planck* the pivot  $k_* = 0.05 \text{ Mpc}^{-1}$  is chosen to decorrelate  $n_s$  and  $\alpha_s$ . For this reason, we considered two additional values of  $k_*$  in the analysis of the “base” ( $\Lambda\text{CDM} + \alpha_s + \beta_s$ ) model with *Planck* ( $TT$ ,  $TE$ ,  $EE$  + lowP) data:  $k_* = 0.01 \text{ Mpc}^{-1}$  and  $k_* = 0.002 \text{ Mpc}^{-1}$ . We report the results in Figs. 8, 9 and Tab. II: we see that at  $k_* = 0.01 \text{ Mpc}^{-1}$  the tilt and  $\beta_s$  decorrelate, while the degeneracy between  $\alpha_s$  and  $\beta_s$  goes from positive to negative. For  $k_* = 0.002 \text{ Mpc}^{-1}$ , instead, we see that  $\alpha_s$  and  $\beta_s$  are still negatively correlated, while the degeneracy between  $n_s$  and  $\beta_s$  becomes positive. However we see from Tab. II that, while changing the pivot cancels the  $1\sigma$  indication for  $\alpha_s > 0$ , the  $2\sigma$  preference for  $\beta_s > 0$  remains in both cases.

We can understand why the marginalized error on  $\beta_s$  does not change if we change the pivot scale  $k_*$  with a simple Fisher analysis. For a log-likelihood for  $\mathbf{n} \equiv (n_s, \alpha_s, \beta_s)$  (marginalized over all parameters except  $n_s, \alpha_s, \beta_s$ ) given by

$$\mathcal{L}|_{k_*^{(0)}} \propto (\mathbf{n} - \mathbf{n}_0)^T \cdot F_{k_*^{(0)}} \cdot (\mathbf{n} - \mathbf{n}_0), \quad (7)$$

with inverse covariance matrix  $F_{k_*^{(0)}}$ , a change of pivot will result in

$$\mathcal{L}|_{k_*} \propto (M \cdot \mathbf{n} - \mathbf{n}_0)^T \cdot F_{k_*^{(0)}} \cdot (M \cdot \mathbf{n} - \mathbf{n}_0), \quad (8)$$

where  $M$  is given by the scale dependence of  $\mathbf{n}$ , *i.e.*

$$\begin{aligned} \mathbf{n}_{k_*} &= M \cdot \mathbf{n}_{k_*^{(0)}} \\ &= \begin{pmatrix} 1 & \log \frac{k_*}{k_*^{(0)}} & \frac{1}{2} \log^2 \frac{k_*}{k_*^{(0)}} \\ 0 & 1 & \log \frac{k_*}{k_*^{(0)}} \\ 0 & 0 & 1 \end{pmatrix} \begin{pmatrix} n_s(k_*^{(0)}) \\ \alpha_s(k_*^{(0)}) \\ \beta_s(k_*^{(0)}) \end{pmatrix}, \end{aligned} \quad (9)$$

and it is straightforward to verify that it has unit determinant. For a Gaussian likelihood, we can forget about  $\mathbf{n}_0$  (we can just call  $\mathbf{n}_0 = M \cdot \mathbf{m}_0$  and do a translation), so that all information will be coming from the transformed inverse covariance, *i.e.*

$$F_{k_*} = M^T \cdot F_{k_*^{(0)}} \cdot M. \quad (10)$$

Since  $M$  has unit determinant, the “figure of merit” f.o.m.  $\propto 1/\det F_{k_*}$  (which is basically  $1/\text{volume}$  of 68% CL ellipsoid) will not change if we change the pivot. What will indeed change are the marginalized and non-marginalized  $1\sigma$  errors on the parameters: however, it is straightforward to show with linear algebra that the marginalized error on the running of the running, which is given by

$$\sigma(\beta_s(k_*)) = \sqrt{\left(F_{k_*}^{-1}\right)_{33}}, \quad (11)$$

does not change under the transformation of Eq. (9).

This simple picture does not explain why the mean values of  $n_s$  and  $\alpha_s$  change. We ascribe this to the presence of the additional parameter  $A_s$ : under the transformation of Eq. (9) it will not change linearly, so the Gaussian approximation will not hold. The data will still constrain  $A_s$  well enough, so that  $\sigma(A_s)$  will not contribute to the errors on the parameters, but the position of the peak of the transformed likelihood will change.

### B. $\Delta\chi^2$ : base model vs. extensions

In this appendix we collect the full  $\Delta\chi^2$  tables: we refer to Sec. III for a discussion of the various improvements and non-improvements in  $\chi^2$  for the different choices of datasets and parameters that have been considered. In all the tables below,  $\Delta\chi^2$  stands for  $\chi_{\text{base}}^2 - \chi_{\text{base} + \text{ext.}}^2$ , both obtained via MCMC sampling of the likelihood.

### C. Derivation of slow-roll expansion for $\epsilon$

Starting from Eq. (5b), differentiating it w.r.t.  $N$  and then using Eq. (5a), one can find the coefficients  $\epsilon^{(i)}$  of a Taylor expansion of  $\epsilon(N)$  in terms of the parameters describing the scale dependence of the primordial spectrum

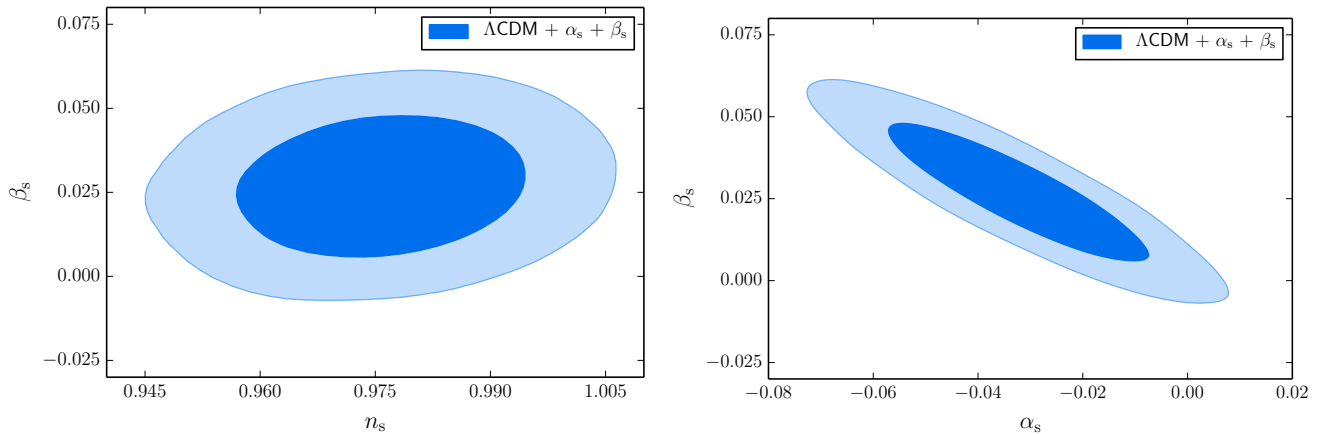


FIG. 8. Likelihood constraints in the  $n_s - \beta_s$  (left panel) and  $\alpha_s - \beta_s$  (right panel) planes for *Planck* ( $TT$ ,  $TE$ ,  $EE$  + lowP), at a pivot  $k_* = 0.01 \text{ Mpc}^{-1}$ .

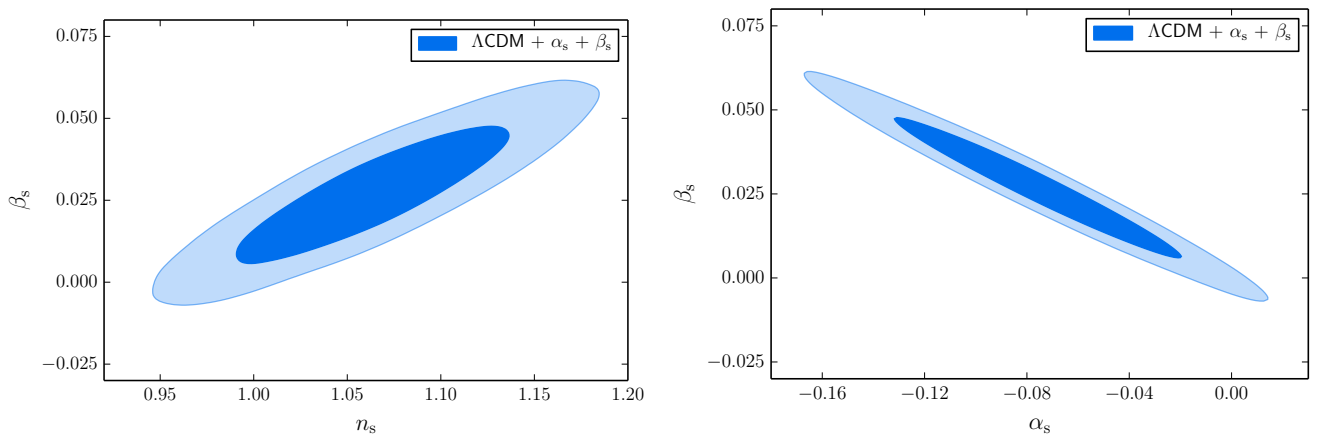


FIG. 9. Likelihood constraints in the  $n_s - \beta_s$  (left panel) and  $\alpha_s - \beta_s$  (right panel) planes for *Planck* ( $TT$ ,  $TE$ ,  $EE$  + lowP), at a pivot  $k_* = 0.002 \text{ Mpc}^{-1}$ .

	vs. $+A_L$	vs. $+\sum m_\nu$	vs. $+\Omega_K$
$\Delta\chi^2_{\text{plik}}$	2.1	-1.8	2.4
$\Delta\chi^2_{\text{lowP}}$	-0.9	-0.6	-1.3
$\Delta\chi^2_{\text{prior}}$	-1.0	0.1	-1.9
$\Delta\chi^2$	0.2	-2.3	-0.7

TABLE VII.  $\chi^2$  comparison between the base  $\Lambda\text{CDM} + \alpha_s + \beta_s$  model and the other extensions considered in the main text, for the *Planck*  $TT$ ,  $TE$ ,  $EE$  + lowP dataset. The last line contains the overall  $\Delta\chi^2$  for all the likelihoods included in the analysis.

	vs. $+A_L$	vs. $+\sum m_\nu$	vs. $+\Omega_K$
$\Delta\chi^2_{\text{plik}}$	1.9	-0.5	1.5
$\Delta\chi^2_{\text{lowP}}$	-0.5	0.1	0.0
$\Delta\chi^2_{\text{prior}}$	-3.8	-2.7	-0.1
$\Delta\chi^2_{\text{lensing}}$	0.9	1.5	-1.3
$\Delta\chi^2$	-1.6	-1.6	0.1

TABLE VIII. Same as Tab. VII, but with the addition of CMB lensing data.

	vs. $+A_L$	vs. $+\sum m_\nu$	vs. $+\Omega_K$
$\Delta\chi_{\text{plik}}^2$	3.0	-4.3	-1.6
$\Delta\chi_{\text{lowP}}^2$	-0.3	0.8	-0.3
$\Delta\chi_{\text{prior}}^2$	0.8	2.9	0.1
$\Delta\chi_{\text{CFHTLenS}}^2$	2.3	-0.6	3.8
$\Delta\chi^2$	5.9	-1.3	2.0

TABLE IX. Same as Tab. VII: the dataset is *Planck TT, TE, EE* + lowP + WL.

	vs. $+A_L$	vs. $+\sum m_\nu$	vs. $+\Omega_K$
$\Delta\chi_{\text{plik}}^2$	0.7	1.0	-2.7
$\Delta\chi_{\text{lowP}}^2$	-1.8	-1.2	-1.0
$\Delta\chi_{\text{prior}}^2$	1.4	0.3	0.8
$\Delta\chi_{\text{6DF}}^2$	0.1	0.0	0.1
$\Delta\chi_{\text{MGS}}^2$	-0.8	0.0	-0.8
$\Delta\chi_{\text{DR11CMass}}^2$	0.9	0.1	1.1
$\Delta\chi_{\text{DR11LOWZ}}^2$	1.1	0.1	1.1
$\Delta\chi^2$	1.5	0.3	-1.4

TABLE X.  $\Delta\chi^2$  for the *Planck TT, TE, EE* + lowP + BAO dataset.

$\Delta_\zeta^2(k)$ . More precisely, one finds (calling  $\epsilon_\star \equiv \epsilon(N_\star)$ )

$$\epsilon^{(1)} = (n_s - 1)\epsilon_\star + 2\epsilon_\star^2, \quad (12a)$$

$$\epsilon^{(2)} = -\alpha_s\epsilon_\star + 4\epsilon_\star\epsilon^{(1)} + (n_s - 1)\epsilon^{(1)}, \quad (12b)$$

$$\begin{aligned} \epsilon^{(3)} = & \beta_s\epsilon_\star - 2\alpha_s\epsilon^{(1)} \\ & + (n_s - 1)\{-\alpha_s\epsilon_\star + 4\epsilon_\star\epsilon^{(1)} + (n_s - 1)\epsilon^{(1)}\} \\ & + 4\{\epsilon_\star[-\alpha_s\epsilon_\star + 4\epsilon_\star\epsilon^{(1)} + (n_s - 1)\epsilon^{(1)}] + (\epsilon^{(1)})^2\}. \end{aligned} \quad (12c)$$

By plugging in the values of  $\alpha_s$  and  $\beta_s$  allowed by *Planck*, one can extrapolate  $\epsilon$  at scales different from  $k_\star$ . See Sec. V for a discussion.

- 
- [1] P. A. R. Ade *et al.* [Planck Collaboration], [arXiv:1502.01589](#) [astro-ph.CO].
- [2] P. A. R. Ade *et al.* [Planck Collaboration], [arXiv:1502.02114](#) [astro-ph.CO].
- [3] E. Calabrese, A. Slosar, A. Melchiorri, G. F. Smoot and O. Zahn, Phys. Rev. D **77**, 123531 (2008) [[arXiv:0803.2309](#) [astro-ph]].
- [4] E. Di Valentino, A. Melchiorri and J. Silk, Phys. Rev. D **93** (2016) no.2, 023513 [[arXiv:1509.07501](#) [astro-ph.CO]].
- [5] Z. Huang, Phys. Rev. D **93** (2016) no.4, 043538 [[arXiv:1511.02808](#) [astro-ph.CO]].
- [6] M. Gerbino, E. Di Valentino and N. Said, Phys. Rev. D **88** (2013) no.6, 063538 [[arXiv:1304.7400](#) [astro-ph.CO]].
- [7] J. B. Muñoz, D. Grin, L. Dai, M. Kamionkowski and E. D. Kovetz, Phys. Rev. D **93** (2016) no.4, 043008 [[arXiv:1511.04441](#) [astro-ph.CO]].
- [8] F. Couchot, S. Henrot-Versillé, O. Perdereau, S. Plaszczynski, B. R. d'Orfeuille and M. Tristram, [arXiv:1510.07600](#) [astro-ph.CO].
- [9] G. E. Addison, Y. Huang, D. J. Watts, C. L. Bennett, M. Halpern, G. Hinshaw and J. L. Weiland, Astrophys. J. **818** (2016) no.2, 132 [[arXiv:1511.00055](#) [astro-ph.CO]].
- [10] E. Di Valentino, A. Melchiorri and J. Silk, Phys. Rev. D **92** (2015) no.12, 121302 [[arXiv:1507.06646](#) [astro-ph.CO]].
- [11] M. Escudero, H. Ramírez, L. Boubekeur, E. Giusarma and O. Mena, JCAP **1602** (2016) no.02, 020 [[arXiv:1509.05419](#) [astro-ph.CO]].
- [12] Q. G. Huang, K. Wang and S. Wang, [arXiv:1512.07769](#) [astro-ph.CO].
- [13] B. A. Powell, [arXiv:1209.2024](#) [astro-ph.CO].
- [14] A. Lewis and S. Bridle, Phys. Rev. D **66**, 103511 (2002) [[astro-ph/0205436](#)].
- [15] A. Lewis, Phys. Rev. D **87**, no. 10, 103529 (2013) [[arXiv:1304.4473](#) [astro-ph.CO]].
- [16] N. Aghanim *et al.* [Planck Collaboration], [[arXiv:1507.02704](#) [astro-ph.CO]].
- [17] P. A. R. Ade *et al.* [Planck Collaboration], [arXiv:1502.01591](#) [astro-ph.CO].
- [18] C. Heymans *et al.*, Mon. Not. Roy. Astron. Soc. **427**, 146 (2012) [[arXiv:1210.0032](#) [astro-ph.CO]].
- [19] T. Erben *et al.*, Mon. Not. Roy. Astron. Soc. **433**, 2545 (2013) [[arXiv:1210.8156](#) [astro-ph.CO]].
- [20] T. D. Kitching *et al.* [CFHTLenS Collaboration], Mon. Not. Roy. Astron. Soc. **442**, no. 2, 1326 (2014) [[arXiv:1401.6842](#) [astro-ph.CO]].
- [21] F. Beutler *et al.*, Mon. Not. Roy. Astron. Soc. **416**, 3017 (2011) [[arXiv:1106.3366](#) [astro-ph.CO]].

- [22] A. J. Ross, L. Samushia, C. Howlett, W. J. Percival, A. Burden and M. Manera, *Mon. Not. Roy. Astron. Soc.* **449**, no. 1, 835 (2015) [[arXiv:1409.3242](#) [astro-ph.CO]].
- [23] L. Anderson *et al.* [BOSS Collaboration], *Mon. Not. Roy. Astron. Soc.* **441**, no. 1, 24 (2014) [[arXiv:1312.4877](#) [astro-ph.CO]].
- [24] M. Cortes, A. R. Liddle and P. Mukherjee, *Phys. Rev. D* **75**, 083520 (2007) [[astro-ph/0702170](#)].
- [25] A. R. Liddle, *Mon. Not. Roy. Astron. Soc.* **351**, L49 (2004) [[astro-ph/0401198](#)].
- [26] M. Gerbino, M. Lattanzi and A. Melchiorri, *Phys. Rev. D* **93** (2016) no.3, 033001 [[arXiv:1507.08614](#) [hep-ph]].
- [27] Y. B. Zeldovich and R. A. Sunyaev, *Astrophys. Space Sci.* **4**, 301 (1969).
- [28] R. A. Sunyaev and Y. B. Zeldovich, *Astrophys. Space Sci.* **7**, 20 (1970).
- [29] J. B. Dent, D. A. Easson and H. Tashiro, *Phys. Rev. D* **86**, 023514 (2012) [[arXiv:1202.6066](#) [astro-ph.CO]].
- [30] J. Chluba, A. L. Erickcek and I. Ben-Dayan, *Astrophys. J.* **758**, 76 (2012) [[arXiv:1203.2681](#) [astro-ph.CO]].
- [31] R. Khatri and R. A. Sunyaev, *JCAP* **1306**, 026 (2013) [[arXiv:1303.7212](#) [astro-ph.CO]].
- [32] S. Clesse, B. Garbrecht and Y. Zhu, *JCAP* **1410**, no. 10, 046 (2014) [[arXiv:1402.2257](#) [astro-ph.CO]].
- [33] K. Enqvist, T. Sekiguchi and T. Takahashi, [[arXiv:1511.09304](#) [astro-ph.CO]].
- [34] G. Cabass, A. Melchiorri and E. Pajer, [[arXiv:1602.05578](#) [astro-ph.CO]].
- [35] J. Chluba, [[arXiv:1603.02496](#) [astro-ph.CO]].
- [36] J. Silk, *Astrophys. J.* **151**, 459 (1968).
- [37] P. J. E. Peebles and J. T. Yu, *Astrophys. J.* **162**, 815 (1970).
- [38] N. Kaiser, *Mon. Not. Roy. Astron. Soc.* **202**, 1169 (1983).
- [39] W. Hu and J. Silk, *Phys. Rev. D* **48**, 485 (1993).
- [40] J. Chluba, R. Khatri and R. A. Sunyaev, *Mon. Not. Roy. Astron. Soc.* **425**, 1129 (2012) [[arXiv:1202.0057](#) [astro-ph.CO]].
- [41] E. Pajer and M. Zaldarriaga, *JCAP* **1302**, 036 (2013) [[arXiv:1206.4479](#) [astro-ph.CO]].
- [42] E. Pajer and M. Zaldarriaga, *Phys. Rev. Lett.* **109**, 021302 (2012) [[arXiv:1201.5375](#) [astro-ph.CO]].
- [43] D. J. Fixsen, E. S. Cheng, J. M. Gales, J. C. Mather, R. A. Shafer and E. L. Wright, *Astrophys. J.* **473**, 576 (1996) [[astro-ph/9605054](#)].
- [44] A. Kogut *et al.*, *JCAP* **1107**, 025 (2011) [[arXiv:1105.2044](#) [astro-ph.CO]].
- [45] J. Chluba and D. Jeong, *Mon. Not. Roy. Astron. Soc.* **438**, no. 3, 2065 (2014) [[arXiv:1306.5751](#) [astro-ph.CO]].
- [46] R. Khatri and R. A. Sunyaev, *JCAP* **1209**, 016 (2012) [[arXiv:1207.6654](#) [astro-ph.CO]].
- [47] J. Chluba, *Mon. Not. Roy. Astron. Soc.* **434**, 352 (2013) [[arXiv:1304.6120](#) [astro-ph.CO]].
- [48] C. Destri, H. J. de Vega and N. G. Sanchez, *Phys. Rev. D* **78**, 023013 (2008) [[arXiv:0804.2387](#) [astro-ph]].
- [49] T. Kobayashi and F. Takahashi, *JCAP* **1101**, 026 (2011) [[arXiv:1011.3988](#) [astro-ph.CO]].
- [50] A. R. Liddle, P. Parsons and J. D. Barrow, *Phys. Rev. D* **50**, 7222 (1994) [[astro-ph/9408015](#)].
- [51] W. H. Kinney, *Phys. Rev. D* **66**, 083508 (2002) [[astro-ph/0206032](#)].
- [52] M. Zaldarriaga, L. Hui and M. Tegmark, *Astrophys. J.* **557**, 519 (2001) [[astro-ph/0011559](#)].
- [53] P. Adshead, R. Easther, J. Pritchard and A. Loeb, *JCAP* **1102**, 021 (2011) [[arXiv:1007.3748](#) [astro-ph.CO]].
- [54] N. Palanque-Desabrouille *et al.*, *JCAP* **1511**, no. 11, 011 (2015) [[arXiv:1506.05976](#) [astro-ph.CO]].
- [55] N. Palanque-Desabrouille *et al.*, *Astron. Astrophys.* **559**, A85 (2013) [[arXiv:1306.5896](#) [astro-ph.CO]].